A&A 451, L39–L42 (2006)
DOI: 10.1051/0004-6361:20065158

Astronomy & Astrophysics

Letter to the Editor

Continuous optical monitoring during the prompt emission of GRB 060111B⋆

A. Klotz[1,2], B. Gendre[3], G. Stratta[2,4], J. L. Atteia[4], M. Boër[2], F. Malacrino[4], Y. Damerdji[1,2], and R. Behrend[5]

[1] CESR, Observatoire Midi-Pyrénées (CNRS - UPS), BP 4346, 31028 Toulouse Cedex 04, France
e-mail: klotz@cesr.fr
[2] Observatoire de Haute-Provence, 04870 Saint Michel l'Observatoire, France
[3] IASF - Roma/INAF, via fosso del cavaliere 100, 00133 Roma, Italy
[4] LATT, Observatoire Midi-Pyrénées (CNRS - UPS), 14 avenue E. Belin, 31400 Toulouse, France
[5] Observatoire de Genève, 1290 Sauverny, Switzerland

Received 8 March 2006 / Accepted 28 March 2006

ABSTRACT

Aims. We present the time-resolved optical emission of GRB 060111B during its prompt phase, measured with the TAROT robotic observatory. This is the first time that the optical emission from a gamma-ray burst has been continuously monitored with a temporal resolution of a few seconds during the prompt gamma-ray phase.
Methods. The temporal evolution of the prompt optical emission at the level of several seconds is used to provide a clue to the origin of this emission.
Results. The optical emission was found to decay steadily from our first measure, 28 s after the trigger, in contrast to the gamma-ray emission, which exhibits strong variability at the same time. This behaviour strongly suggests that the optical emission is due to the reverse shock.

Key words. gamma-rays: bursts

1. Introduction

GRB 060111B was a bright, double-peak, gamma-ray burst (GRB) detected on January 11th, 2006, at 20:15:43.24 UT (hereafter $t_{\rm trig}$) by the BAT instrument on the Swift spacecraft (trigger = 176918, Perri et al. 2006; Tueller et al. 2006). The first peak started at $t - t_{\rm trig} = -4$ s, peaked at $t - t_{\rm trig} = +1$, and extended out to $t - t_{\rm trig} = +28$ s. The second, smaller peak started at $t - t_{\rm trig} = +53$, peaked at $t - t_{\rm trig} = +55$, and was over by $t - t_{\rm trig} = 62$ s. The duration T_{90} was 59 ± 1 s in the range 15−350 keV. The power-law index of the time-averaged spectrum ($t_{\rm trig} - 2$ to $t_{\rm trig} + 63$ s) was 1.04 ± 0.17. The fluence in the 15−150 keV band was $(1.6 \pm 0.1) \times 10^{-6}$ erg/cm^2. The 1s peak photon flux measured from $t_{\rm trig} + 0.36$ s in the 15−150 keV band was 1.4 ± 0.3 ph/cm^2/s. No optical redshift was available when this paper was written. Perri et al. (2006) mentions that UVOT detected the afterglow in a filtered B image taken about five minutes after the trigger. If we conservatively place the Lyman alpha limit at the end of the B bandpass (480 nm, Bessel 1990), GRB 060111B is at $z < 3.0$.

In this letter we report early optical observations of GRB 060111B, performed with the TAROT robotic observatory. The gamma-ray burst coordinates network (GCN) notice, providing celestial coordinates to ground stations, was sent at 20:16:03 (Perri et al. 2006). The first image of TAROT started at 20:16:11.22 UT, 27.98 s after the GRB (9 s after the notice) and 34 s before the end of the high-energy emission. From our images, we derived its position: RA = $19^{\rm h}05^{\rm m}42.46^{\rm s}$ and Dec = $+70°22'32.3''$ (J2000.0) with an accuracy of 1 arcsec. The observations presented here provide the first opportunity to check the rapid variability of the optical emission during the prompt phase of a gamma-ray burst.

2. TAROT observations

TAROT is a fully autonomous 25 cm aperture telescope installed at the Calern observatory (Observatoire de la Côte d'Azur – France) devoted to very early observations of GRB optical counterparts. A technical description can be read in Klotz et al. (2005). The first image of GRB 060111B is a 60 s exposure taken in drift mode. The tracking of the hour-angle motor was adapted to a drift of 0.30 pixel/s. As a consequence, stars are trailed with a length of about 18 pixels on the image (see Fig. 1) and the flux was recorded continuously with no dead time. Subsequent images were recorded as a series of 30 s exposures tracked on the diurnal motion. All images were taken with no filter. The on-line pre-processing software provided calibrated images (dark-corrected, flat-fielded and astrometrically calibrated from the USNO-A2.0 catalog). The optical transient is detected in the first 4 images. Subsequent images were co-added to increase the signal-to-noise ratio but the afterglow was not detected.

From the trailed image, the optical light-curve is directly obtained by a binning in the declination direction. We chose USNO-B1 1604-0125526 (R = 13.90) as the reference star for flux calibration. Stars USNO-B1 1603-0125834 (R = 15.79) and 1603-0125830 (R = 16.40) were close to the optical transient,

⋆ Based on observations performed with TAROT at the Calern observatory.

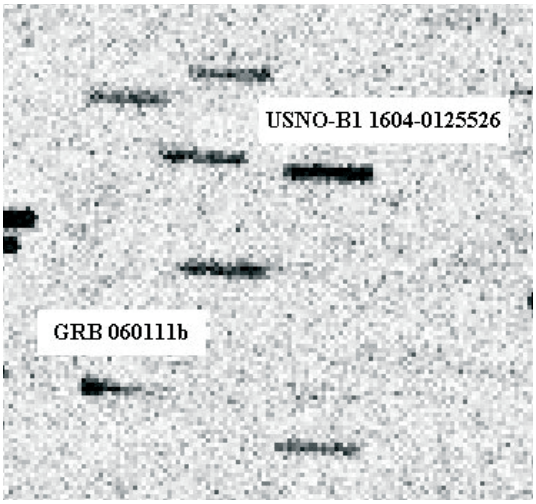

Fig. 1. This image was taken between 28 s and 88 s after the GRB trigger. The hour angle speed was adapted to obtain stars as trails of ∼18 pixel length during the 60 s exposure. The light-curve was then time-resolved with no dead time. In this image, the nearby star USNO-B1 1603-0125834, close to the GRB, was removed using the trail of USNO-B1 1604-0125526.

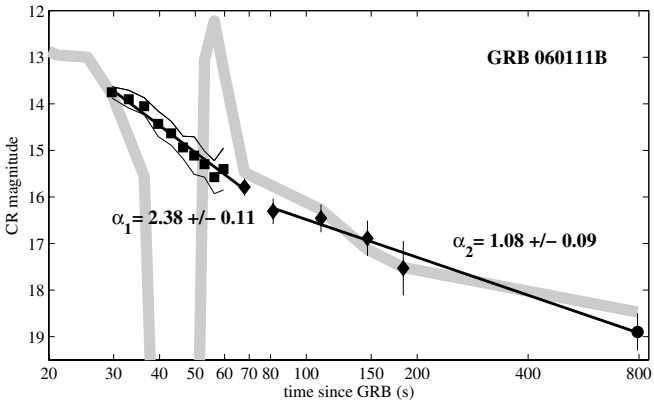

Fig. 2. light-curves of GRB 060111B. Black squares and diamonds with vertical error bars are CR magnitudes measured by TAROT (see Table 1). The black circle indicates the *R* magnitude measured by MITSuME (Yanagisawa et al. 2006). The solid straight lines are fits by a $f(t) \propto t^{-\alpha}$ law. The broad grey line shows the high-energy light-curve (−2.5 log(X-ray flux)) vertically offset to be compared to the optical light-curve. Before 75 s we extrapolated Swift-BAT flux to the 2−10 keV energy range. After 90 s, we used the XRT data in the 2−10 keV energy range (see Table 2).

Table 1. Log of the optical measurements from TAROT. *T* are seconds since $t_{\rm trig}$. Uncertainties on CR magnitudes are 2σ errors.

$T_{\rm start}$	$T_{\rm end}$	CR	$T_{\rm start}$	$T_{\rm end}$	CR
28.0	31.3	13.75 ± 0.12	54.6	58.0	15.58 ± 0.35
31.3	34.6	13.90 ± 0.19	58.0	61.3	15.40 ± 0.45
34.6	38.0	14.05 ± 0.18	61.3	74.6	15.79 ± 0.19
38.0	41.3	14.43 ± 0.27	74.6	87.9	16.31 ± 0.27
41.3	44.6	14.63 ± 0.26	94.6	124.6	16.46 ± 0.30
44.6	48.0	14.94 ± 0.24	131.5	161.5	16.89 ± 0.38
48.0	51.3	15.11 ± 0.40	168.3	198.3	17.53 ± 0.59
51.3	54.6	15.30 ± 0.28			

and were removed by an appropriate scaling of the reference star. From $t_{\rm trig}$ + 28 s to $t_{\rm trig}$ + 61 s, we used a time sampling of one pixel (3.33 s). After 61 s we used a four-pixel time sampling (13.3 s) until the end of the trail to increase the signal-to-noise ratio. For the non-trailed images, we fit the optical transient by the PSF of the reference star to deduce magnitudes. We designated as CR the magnitudes computed from our unfiltered images calibrated with the reference star. Differences between CR and *R* magnitudes come from uncertainties in the calibration of the *R* magnitude of the reference star and from colour differences with the optical transient. Table 1 gives the results. Due to the unknown accuracy of the USNO-B1 catalog, a global shift of ±0.2 mag cannot be excluded.

3. The prompt emission and early afterglow

The optical light-curve of GRB 060111B is presented in Fig. 2. The optical emission exhibits two phases. A fast decaying phase with a slope $\alpha_1 = 2.38 \pm 0.11$ dominates from 28 s to 80 s after the trigger, roughly corresponding to the first TAROT exposure with high temporal resolution. This fast decay was also observed by ROTSE-IIId (Yost et al. 2006b). This phase is followed by a period of shallower decay with a slope $\alpha_2 = 1.08 \pm 0.09$, typical of the late afterglow phase. The observation of Yanagisawa et al. (2006) in the *R* band at $t_{\rm trig}$ + 800 s is compatible with the extrapolation of the TAROT points with this slope. The transition between the two phases occurred at $t_{\rm trig}$ + 80 s, about 20 s after the end of the gamma-ray emission. These slopes and transition time were derived under the assumption that there is a single emission component evolving from a steep to a shallow decay. If we assume instead that the optical emission is due to the superposition of two components that are simultaneously present (e.g. the forward and the reverse shocks), the slopes of the fast and shallow decays become $\alpha_1 = 3.0$ and $\alpha_2 = 0.89$, respectively, and the transition occurs at $t_{\rm trig}$ + 65 s, right at the end of the gamma-ray emission.

A remarkable feature of the prompt optical light-curve is its smoothness. As can be seen in Fig. 2, the broken power-law fit adequately reproduces the evolution of the optical emission from $t_{\rm trig}$ + 28 s to $t_{\rm trig}$ + 200 s. All individual measurements are consistent with a smooth decay of the optical emission. This is the first time that the optical variability of a gamma-ray burst could be measured during the prompt phase[1], down to timescales of ∼5 s. Figure 2 also displays the high-energy light-curve in the 2−10 keV energy range (the broad grey line). Before 75 s, the 2−10 keV flux was extrapolated from the flux measured with the BAT in the 15−150 keV energy range, assuming a spectrum with a photon index $\Gamma = -1.57$, in agreement with the prescription of O'Brien et al. (2006) recommending use of a photon index that is the average of the values measured in the BAT and in the XRT. After 90 s, the 2−10 keV light-curve was measured by the XRT. The high-energy (2−10 keV) fluxes in time intervals that are simultaneous with the optical intervals are given in Table 2. The high-energy emission is highly variable, with two well-defined peaks. The variability of the high-energy emission contrasts with the smoothness of the optical emission observed at the same time. In particular, we note that there is no significant variation in the optical flux at the time of the second gamma-ray peak at $t_{\rm trig}$ + 55 s. After $t_{\rm trig}$ + 90 s, the XRT light-curve can be described by a simple power-law with slope 1.1 ± 0.1, which is fully compatible with the slope of the optical emission.

Figure 3 shows the broad-band spectrum of the emission during the early afterglow from $t_{\rm trig}$ + 95 s to $t_{\rm trig}$ + 200 s. The energy

[1] We call "prompt phase" the period during which SWIFT/BAT detected the high-energy emission. This period extended from 2 s before the trigger to 62 s after the trigger.

Table 2. 2−10 keV light-curve of GRB 060111B. Columns 1, 2, 4, and 5 give the start and end times of the intervals in seconds after the trigger. Columns 3 and 6 give the high-energy fluxes and their errors in units of 10^{-10} erg cm^{-2} s^{-1}. Fluxes before $t_{\rm trig}$ + 75 s are based on an extrapolation of the BAT counts to the 2−10 keV range (see text). Fluxes after 90 s are measured by the XRT. All fluxes have been corrected for absorption considering a column density of hydrogen of $N_{\rm H} = 2.8 \times 10^{21}$ cm^{-2}.

$T_{\rm start}$	$T_{\rm end}$	Flux	$T_{\rm start}$	$T_{\rm end}$	Flux
0.1	0.50	190 ± 37	25.3	27.6	45 ± 10
0.50	1.13	260 ± 40	27.6	33.0	22 ± 11
1.13	2.0	210 ± 27	33.0	41.3	4.3 ± 5.3
2.0	3.0	180 ± 27	41.3	49.6	0 ± 4.1
3.0	4.0	120 ± 25	49.6	54.6	43 ± 6.8
4.0	5.25	88 ± 25	54.6	58.0	92 ± 7.0
5.25	7	88 ± 18	58.0	63.8	35 ± 6.5
7	9	80 ± 18	63.8	74.6	4.6 ± 3.2
9	11.5	47 ± 18	94.6	124.6	2.2 ± 0.3
11.5	15	84 ± 12	131.5	161.5	1.0 ± 0.3
15	19	66 ± 12	168.3	198.3	0.7 ± 0.2
19	23.3	47 ± 12	762.0	822.0	0.29 ± 0.09

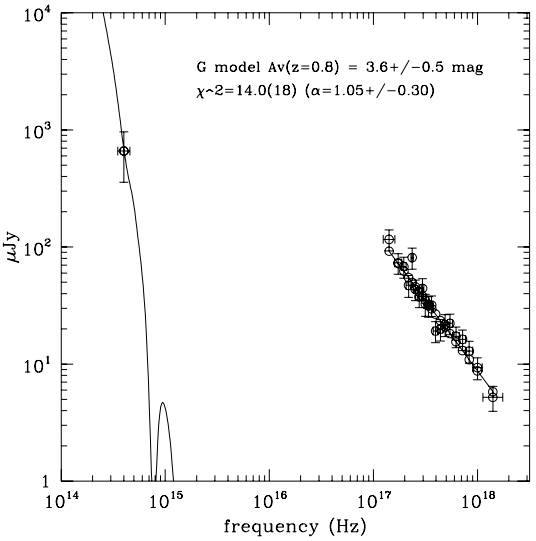

Fig. 3. The optical-to-X-ray afterglow spectrum from 95 s to 198 s after the burst. The X-ray data have been corrected for both the Galactic and the extra-galactic absorption. The optical data have been corrected only from the Galactic extinction. The solid line is the best-fit absorbed power-law model. We assumed a local extinction curve similar to the one observed in our Galaxy. The spectral index was fixed within the errors to the value derived only from the X-ray analysis.

index of the 0.5−10 keV spectrum is 1.05 ± 0.3, a typical value for an afterglow. The X-ray spectrum requires an absorption corresponding to $N_{\rm H} = 2.8 \pm 0.8 \times 10^{21}$ cm^{-2}, significantly exceeding the galactic value, $N_{\rm H} = 0.7 \times 10^{21}$ cm^{-2}. The extrapolation of the unabsorbed X-ray spectrum to the optical range overpredicts the optical emission, indicating the necessity of a break between the optical and X-ray domains. This break could reflect the spectral distribution of the emission or a strong optical extinction. With the data at hand, it is difficult to choose between these two possibilities. Nevertheless if we consider the consistency of the decay rate at optical and X-ray wavelengths as an indication of a common origin, we may attribute the observed spectral break to optical extinction. An extinction of $A_R = 4$ mag is required to reconcile the measured optical flux with the extrapolation of the XRT spectrum. We note that a dense environment could explain many features of GRB 060111B: a reverse shock peaking early (see next section), a large column density of hydrogen, and a possible large optical extinction.

Assuming a standard galactic extinction law, the optical extinction is compatible with the hydrogen column density measured in X-rays ($N_{\rm H}$), if the source is situated at $z \sim 0.8$ (and $A_{\rm v} = 3.6$ at the source). This is the situation illustrated in Fig. 3. Given the errors on the measurement of $N_{\rm H}$, the consistency between the expected and the measured $N_{\rm H}/A_{\rm v}$ ratio is maintained up to $z_{\rm max} = 1.2$. Larger redshifts (up to $z = 2.5$) are also possible if we assume a non-standard extinction law with a weaker wavelength dependence than for the Galactic case (Stratta et al. 2004).

4. Interpretation of the observations

The nature of the optical light contemporaneous with the prompt gamma-ray emission remains an important, yet open, issue. In the internal/external shock model, the prompt optical emission could be due to internal shocks within the relativistic ejecta and/or to the reverse shock crossing the ejecta. In both cases the optical radiation carries crucial information on the composition of the ejecta. This information is lost at later times, when the optical emission is dominated by the afterglow from the external shock. The first step on the (long) way to the comprehension of GRB ejecta is thus to clarify whether the optical emission originates in internal shocks or in the reverse shock. This issue has been discussed for a few GRBs in which the prompt optical emission could be detected, but with diverse conclusions.

The bright optical flare of GRB 990123 (Akerlof et al. 1999) has been attributed to reverse-shock emission (Sari & Piran 1999a; Mészáros & Rees 1999; Wang et al. 2000, and references therein). This interpretation had important implications for the physical properties and composition of the ejecta and of the surrounding medium (e.g. Sari & Piran 1999b; Fan et al. 2002; Zhang et al. 2003). On the other hand, Vestrand et al. (2005) find that the optical emission of GRB 041219A is proportional to the high-energy emission of this burst, which is the behaviour expected if the optical emission is due to internal shocks, although this conclusion is based on three points with a positive detection, which might also be explained by a bright optical flare followed by a steep decay. The case of GRB 050904 is less clear because the optical flare is almost simultaneous with a strong X-ray flare attributed to the prompt emission (Boër et al. 2006; Wei et al. 2006).

The TAROT observations presented here allow a first investigation of the details of the temporal structure of the prompt optical emission, thereby providing crucial data to resolve the question of the origin of this emission. Such a study has not been possible till now, due to the shortness of the bursts (GRB 021211, GRB 050319, GRB 050401, GRB 050801), to a low temporal resolution (GRB 990123), or to the faintness of the optical emission (GRB 041219A and GRB 050904). Our observations reveal the lack of fine time structure during the decay of the bright optical flare of GRB 060111B. This result is particularly significant since, during the same time interval, the gamma-ray light-curve shows a peak not seen in optical observations. The lack of correlation between the optical emission and the high-energy radiation eliminates internal shocks as the main origin of the optical light seen by TAROT. In consequence, the single flash detected by TAROT and ROTSE-IIId must be attributed to the reverse shock or to a forward shock peaking early. The fast decay of the optical emission with $\alpha_1 = 2.4$, strongly suggests that it comes from the reverse shock.

The peak of the forward shock is not detected and must be below the level of the reverse shock emission; this is the type II light-curve studied by Zhang et al. (2003). It is generally assumed that the physical parameters of the reverse shock and of the forward shock are similar (e.g., Sari & Piran 1999a,b; Mészáros & Rees 1999; Wang et al. 2000; Wei 2003). In that case, however, as shown in Zhang et al. (2003) and Fan et al. (2005), the reverse shock optical emission can not dominate over the forward shock optical emission when the latter peaks. It therefore looks surprising that no forward shock peak is evident in the optical lightcurve. Notwithstanding, such a situation has been observed in GRB 990123, GRB 021211, and the current burst GRB 060111B and may be common among GRBs. Such light-curves suggest that the physical parameters in the reverse shock are much larger than in the forward shock, in particular, the fraction of shock energy given to the magnetic field. The thermal energy density contained in both shocks being comparable, the magnetic field in the reverse shock is thus much stronger than the one in the forward shock. Type II light-curves have been used as an indication that the GRB outflow is magnetized (e.g., Fan et al. 2002; Zhang et al. 2003). Detailed simulations of the pan-chromatic emission of GRB 060111B, including the prompt emission, the unambiguously identified reverse shock, and the early forward shock are beyond the scope of this paper; yet it can be expected that such simulations will bring new insight into the nature of GRB ejecta.

Acknowledgements. B.G. and G.S. acknowledge the support by the EU Research and Training Network "Gamma-Ray Bursts, an Enigma and a Tool". The TAROT telescope is funded by the *Centre National de la Recherche Scientifique* (CNRS), *Institut National des Sciences de l'Univers* (INSU), and the Carlsberg Fundation. It was built with the support of the *Division Technique* of INSU. We thank the technical staff contributing to the TAROT project: G. Buchholtz, J. Eysseric, C. Pollas and Y. Richaud. The authors thank the anonymous referee for very helpful comments on the interpretation of the observations.

References

Akerlof, C., Balsano, R., Barthelmy, S., et al. 1999, Nature, 398, 400
Bessel, M. S. 1990, PASP, 102, 1181
Boër, M., Atteia, J.-L., Damerdji, Y., et al. 2006, ApJ, 638, L71
Fan, Y.-Z., Dai, Z.-G., Huang, Y.-F., & Lu, T. 2002, CJAA, 2, 449
Fan, Y. Z., Zhang, B., & Wei, D. M. 2005, ApJ, 628, L25
Klotz, A., Boër, M., Atteia, J. L., et al. 2005, A&A, 439, L35
Mészáros, P., & Rees, M. J. 1999, MNRAS, 306, L39
O'Brien, P. T., Willingale, R., Osborne, J., et al. 2006, ApJ, submitted [arXiv:astro-ph/0601125]
Perri, M., Barthelmy, S., Boyd, P., et al. 2006, GCNC, 4487
Sari, R., & Piran, T. 1999a, ApJ, 517, L109
Sari, R., & Piran, T. 1999b, ApJ, 520, 641
Stratta, G., Fiore, F., Antonelli, L. A., et al. 2004, ApJ, 608, 846
Tueller, J., Barbier, L., Barthelmy, S., et al. 2006, GCNC, 4492
Vestrand, W. T., Wozniak, P. R., Wren, J. A., et al. 2005, Nature, 435, 178
Wang, X. Y., Dai, Z. G., & Lu, T. 2000, MNRAS, 319, 1159
Wei, D. M. 2003, A&A, 402, L9
Wei, D. M., Yan, T., & Fan, Y. Z. 2006, ApJ, 636, L69
Yanagisawa, K., Toda, H., & Kawai, N. 2006, GCNC, 4496
Yost, S. A., Yuan, F., Swan, H., et al. 2006b, GCNC, 4488
Zhang, B., Kobayashi, S., & Meszaros, P. 2003, ApJ, 595, 950